

The impact of metallic contacts on spin-polarized photocurrents in topological insulator Bi₂Se₃ nanowires

N. Meyer,¹ K. Geishendorf,² J. Walowski,¹ A. Thomas,² and M. Münzenberg¹

¹*Institute of Physics, University of Greifswald, Felix-Hausdorff-Str. 6, 17489 Greifswald, Germany*

²*IFW Dresden, Institute for Metallic Materials, Helmholtzstraße 20, 01069 Dresden, Germany*

(Dated: 8 June 2022)

Recently, a new quantum phase, the topological insulator, has been vividly investigated in a variety of materials. Its unique bandstructure allows for optical generation and control of spin-polarized currents based on the circular photogalvanic effect. In this paper, we generate and distinguish the different photocurrent contributions via the polarization of the driving light wave. We discuss the helicity-dependent spin-polarized current and the polarization independent thermoelectric current as spatially resolved maps, focusing on the influence of the topological insulator/metallic contact interface. We observe for both current contributions a significant enhancement of the current values at the topological insulator/metallic contact interface and moreover a dipole-like distribution of the spin-polarized current close to the contacts. We discuss the general behavior of the thermovoltage as a three-material Seebeck effect and explain the enhanced values by the acceleration of the photoelectrons generated in the space charge region of the topological insulator/metallic contact interface. Furthermore, we interpret the temperature gradient together with the spin Nernst effect as a possible origin for the enhancement and dipole-like distribution of the spin-polarized current.

Recently, topological order gained a lot of attention among physicists after the discovery of topological insulators (TIs)^{1–3} in solid state materials. This additional state of quantum matter differs from trivial insulators by hosting a bulk energy gap, while the surface possesses gapless electronic states that are protected by time-reversal symmetry. The spin-momentum locking present in TIs suppresses the backscattering of the surface states in the absence of magnetic impurities^{4,5} making them promising candidates for spintronics- or optoelectronics applications. In this paper, we investigate Bi₂Se₃, which, among Bi₂Te₃ and Sb₂Te₃, belongs to the "second generation" of TIs^{6,7}. The non-trivial topology of this group of strong topological insulators is caused by a band inversion due to the large SOC in the p-orbital manifold at the Γ -point⁵. The topologically-protected surface states make those materials suitable candidates for polarization-sensitive detectors based on the polarization-dependent photovoltaic and photogalvanic effects^{8,9}. The underlying idea for polarization-sensitive detectors is creating an asymmetric distribution of spin-polarized surface states which gives rise - due to the spin-momentum locking - to a directed spin-polarized current. The physical mechanism behind the optically induced asymmetric surface state distribution is the circular photogalvanic effect (CPGE) which was first established in semiconductor quantum wells¹⁰. This idea has been realized in several optoelectronic experiments, which demonstrate the direction control of spin-polarized currents by circular polarized light on TI materials structured to devices in the micrometer range^{11–13}. But only little is known about those effects when the dimensions of TIs decrease towards the nanometer scale e.g. in nanowires. There is one example for all-optical control in Bi₂Te₃Se nanowires by Seifert et al.¹³, who

observe an enhancement of the THz amplitude in the vicinity of the gold contacts which they explain by a locally enhanced spin-polarized current. Hence the goal in this paper is to measure the spatial distribution of spin-polarized currents across TI nanowire devices to further investigate the influence of the metallic contacts on the spin-polarized current and to discuss the origin of their enhancement close to the topological insulator/metallic contact interface.

The photoelectric measurements in this paper are performed on Bi₂Se₃ nanowires synthesized by the gold-catalyzed vapor-liquid-solid method (for more details on the nanowire growth see Shin et al.¹⁴). The nanowires are grown in [110] direction as single-crystal structures assuring a smooth surface. The nanowire dimensions are larger than 10 nm to prevent hybridization of the topological surface states^{14,15}. The width is in the order of 50 nm and the thickness spans from 50 nm to 150 nm. The nanowires are transferred mechanically to a Si(111) substrate with 100 μm of SiO_x. Contact pads of 5 nm Cr underneath 50 nm Au are subsequently patterned above for electric contact. The contact spacing is 14 μm . The nanowire devices for each measurement are displayed in a micrograph (see FIG. 2(a) and FIG. 3(c) and (f)). The photoelectric measurements are recorded using the lock-in technique. A diode laser with a wavelength of 785 nm (1.55 eV) modulated at 77 Hz by a square-function generator serves as a light source. The laser beam is guided through a linear polarizer combined with a rotatable quarter-wave plate (qwp) for polarization control before impinging at an angle of incidence of $\theta = 45^\circ$ on the sample surface. The laser light is focused down to a spot size of $(2.9 \pm 0.08) \mu\text{m} \times (3.4 \pm 0.12) \mu\text{m}$ on the sample surface. The measured photocurrent $j(\alpha)$ (photovoltage $v(\alpha)$) is mapped to the polarization state via the qwp

rotational angle α . Thus, the photocurrent is measured at fixed positions (k,j) for linear, left-circular and right-circular polarized light, scanning the sample surface vertically and horizontally by moving the laser across the sample surface with stepper motors. At the same time, the light intensity $I(\alpha)$ reflected from the sample surface is recorded by a second lock-in amplifier via a photodiode for each rotational angle α . The qwp rotates at every laser spot position (k,j) from $\alpha = 0, \Delta\alpha, \dots, 360^\circ$ with a step size of $\Delta\alpha = 6^\circ$. Afterwards, the laser spot is moved in the vertical direction by $\Delta j = 1 \mu\text{m}$ to the next position $(k, j - \Delta j)$. There, the qwp is again rotated and the photocurrent $j(\alpha)$ and the reflected intensity $I(\alpha)$ are measured. This generates a set of 60 current (voltage) values at each position (j,k) as presented in FIG. 1. The photocurrent (voltage) is measured until the last position $(0,0)$ is reached.

The data is evaluated by identifying the contributions in the measured photocurrent (voltage) by their polarization dependence. We use the ansatz suggested by McIver et al.¹¹ that includes four contributions:

$$j(\alpha) = C \sin(2\alpha) + L_1 \sin(4\alpha) + L_2 \cos(4\alpha) + D. \quad (1)$$

In our measurements, the laser light is linear polarized at $\alpha = 0, 90, 180, 270$ and 360° , left-circular polarized σ^+ at $\alpha = 45$ and 225° and right-circular polarized σ^- at $\alpha = 135$ and 345° . The term $C \sin(2\alpha)$ in Eq.(1) represents the spin-polarized helicity dependent current. The amplitude $2C$ is the photocurrent difference between σ^+ - and σ^- -light. The qwp phase is set so that $\sin(2\alpha)$ is zero for linear polarized light. The physical origin of this term is still under discussion. Measurements by Shalgyin et al. on (110)-grown quantum wells prove that the circular photon drag effect can cause a helicity-dependent current¹⁶, while later measurements on exfoliated Bi₂Se₃ Hall bar devices by McIver et al.¹¹ related the helicity-dependent currents to the CPGE. In this paper, we relate the first term $C \sin(2\alpha)$ in Eq. (1) to the CPGE following the notation established in the recent works^{11,17} and discuss the amount of spin-polarized current by displaying the amplitude C . Both middle terms, $L_1 \sin(4\alpha)$ and $L_2 \cos(4\alpha)$, have a different frequency than the first term, hence they do not affect the first term. The third term $L_2 \cos(4\alpha)$ represents the polarization-dependent absorption. The physical effects related to the two contributions are still under discussion both being sometimes related to the linear photogalvanic effect or the photon drag effect^{11,18,19}. The last term D is polarization independent. As we have shown in a previous work by ref.²⁰, the physical origin is the Seebeck effect. Additional contributions caused by the polarization-independent photogalvanic or photon drag effects are negligible.

For data analysis, the function $j(\alpha)$ ($v(\alpha)$) is fitted to the experimental data to extract the parameters C , L_1 , L_2 and D at each position (j,k) as in FIG. 1. The discussed parameters C and D are displayed in two dimensional maps as a function of the laser spot position, see FIG. 2(b) and (c). The contact pad positions (edges are

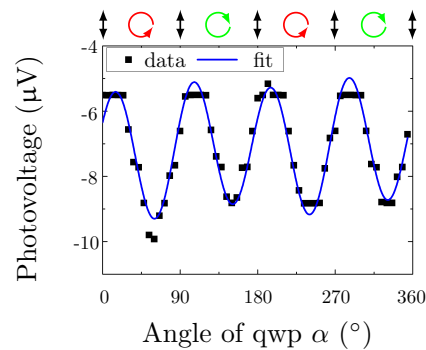


FIG. 1. Measured photovoltage $v(\alpha)$ for $\alpha = 0, \Delta\alpha, \dots, 360$ with $\Delta\alpha = 6^\circ$ at position (17,8) in FIG. 3(d). The measured data (black squares) and the fit function (blue line) are displayed. The top arrows represent the polarization state of the laser light.

marked by orange lines) and the nanowire (black line) are determined from reflectivity data. We concentrate on the parameters C and D to investigate the influence of the thermoelectric current on the spin-polarized photocurrent and their apparent enhancement in the vicinity of the contact pads.

The two dimensional map of the thermoelectric current in FIG. 2(b) shows that the thermoelectric current changes its sign when the laser spot is moved from one contact to the other. The contour plot (green line in FIG. 2(b)) along the nanowire demonstrates that the slope of the thermoelectric current changes along the nanowire and the thermoelectric current reaches its extremal values at the crossing of the contact pads and the nanowire. The pink and grey contour plots extracted along the contact pads emphasize this by indicating that the temperature gradient along the nanowire is not constant. The current map of the spin-polarized current, represented by the parameter C , is displayed in FIG. 2(c). We find a constant spin-polarized current along the nanowire in a small area where the contact pads can be neglected. When the laser spot illuminates the nanowire close to the contact pads, the spin-polarized current increases and shows a dipole-like distribution. We observed the same distribution in an earlier work see ref²⁰.

The measurement was repeated on a second nanowire, maintaining the contact distance and laser conditions, but changing the contact geometry. The results for axisymmetric contacts or point-symmetric contacts are shown in FIG. 3. For the thermoelectric contribution, we observe for both contact geometries enhanced values at the crossing of the contacts and the nanowire. The thermovoltage in FIG.3(a) reaches $D = 15.13 \mu\text{V}$ at the drain electrode and goes down to $D = 0.85 \mu\text{V}$ at position (12,7) on the nanowire, which qualitatively matches the findings for the thermoelectric current in FIG.2. In FIG.3(b) and (e), the spin-polarized voltages for the two contact geometries are displayed. The spin-polarized voltage reaches a minimum of $C = -1.84 \mu\text{V}$

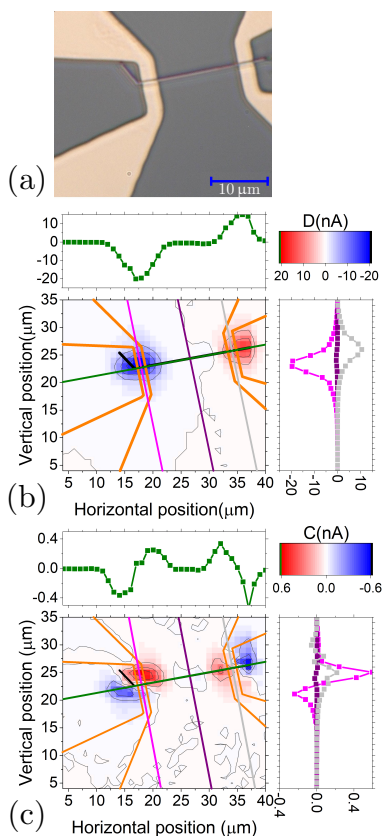


FIG. 2. Photocurrent measurement on a Bi_2Se_3 nanowire with a $14\ \mu\text{m}$ gap with the drain (source) electrode on the right (left). (a) shows the micrograph of the measured area. The spatially resolved results for (b) the thermoelectric current and (c) the spin-polarized current are presented, including contour plots along the nanowire (green lines), the contacts (pink and gray lines) and through the center of the nanowire (violet lines).

at (22,8) close to the source electrode and decreases to $C = -0.52\ \mu\text{V}$ at (14,8) in the middle of the nanowire. At the crossing of the contact pad and the nanowire, the voltage is dipole-like distributed, which is in good agreement with the results observed in FIG.2(c). Switching between the axisymmetric and the point-symmetric contacts does not affect the shape of the distribution or the sign of the voltage at different areas (see FIG. 3(b) and (e)). We find a dipole-like distributed spin-polarized current for different nanowires.

In the following we will discuss the origin of the sign change of the thermovoltage along the nanowire and the enhancement of the thermovoltage at the nanowire/contact interface. The thermovoltage ΔV along the nanowire is caused by the local heating by the laser light. This can be described with a simple qualitative model based on the Seebeck effect. For simplicity, we omit the 5 nm thick chromium interlayer and treat the contacts as a pure gold layer. Leonard et al. observed in a device of two metal contacts and a semiconductor nanowire an en-

hanced thermovoltage²¹ which matches our results qualitatively. According to them, the thermovoltage ΔV for our simplified device can be written as

$$\Delta V = V_D - V_s = (S_{Au} - S_{TI})(T_D - T_S) \quad (2)$$

where S_{Au} is the Seebeck coefficient of the gold contact, S_{TI} is nanowire Seebeck coefficient, T_D is the drain temperature (ground electrode), and T_S is the source temperature (minus pole). We have $S_{Au} - S_{TI} > 0$ in Eq.(2), since the Seebeck coefficient for gold is $S_{Au} = 1.94\ \mu\text{V}/\text{K}$ at 300 K and for Bi_2Se_3 nanowires is $S_{TI} \approx 100\ \mu\text{V}/\text{K}$ at 300 K¹⁴. When the drain electrode is illuminated, we get $T_D > T_S$ which results in a positive thermovoltage ΔV . This is in good agreement with FIG. 3(d). Illuminating the source electrode would reverse the voltage which matches the results in FIG. 3(d). Changing the contact geometry from axisymmetric to point-symmetric (see FIG.3(a)) does not effect the temperature gradient. Hence, the results in FIG. 3(a) and (f) are the same.

The simple model for the two-interface Seebeck effect in Eq. (2) describes the sign change of the thermovoltage along the nanowire, but an additional effect is needed to explain the thermovoltage enhancement at the nanowire/contact interface. The band gap of Bi_2Se_3 is 300 eV which is typical for semiconductors. Therefore, we expect a band bending at the interface depicted in FIG.3(g). Due to the band bending, a positive (negative) space charge zone forms in the contact (nanowire) at the interface. When the laser illuminates the nanowire close to the contact near the drain electrode, an electron-hole pair is created. The electron will be accelerated to the drain electrode and the hole to the center of the nanowire, driven by the electric field around the interface. The electrons entering the drain electrode will contribute to the net-positive current when the holes annihilate with electrons, originating from the source electrode. The photoelectrons generated close to the source electrode contribute to the net-negative current, since the electric field of the space charge region changes its sign. The enhancement at the drain electrode has a maximum at position (7,7) and decreases when the laser spot is moved away from this position. The decrease is due to the Gaussian laser intensity profile. When the laser spot is moved away from position (7,7), less photons illuminate the contact/nanowire interface and the current contributing to the measured voltage decreases. The same effect appears at the source electrode, but with an opposite sign.

Comparing the position of the extremal spin-polarized voltage in FIG.3(e) reveals that the largest and smallest spin-polarized current are located at the edges of the contacts. This is similar to our earlier observations²² on photocurrent measurements on $(\text{Bi}_{0.57}\text{Sb}_{0.43})_2\text{Te}_3$ Hall bars. There we report the accumulation of a negative spin-polarized current along one Hall bar edge and a positive spin-polarized current along the opposite edge, caused by the spin Nernst effect. The spin Nernst effect leads to an additional movement of spin-up and spin-down electrons in opposite directions perpendicular to the temperature

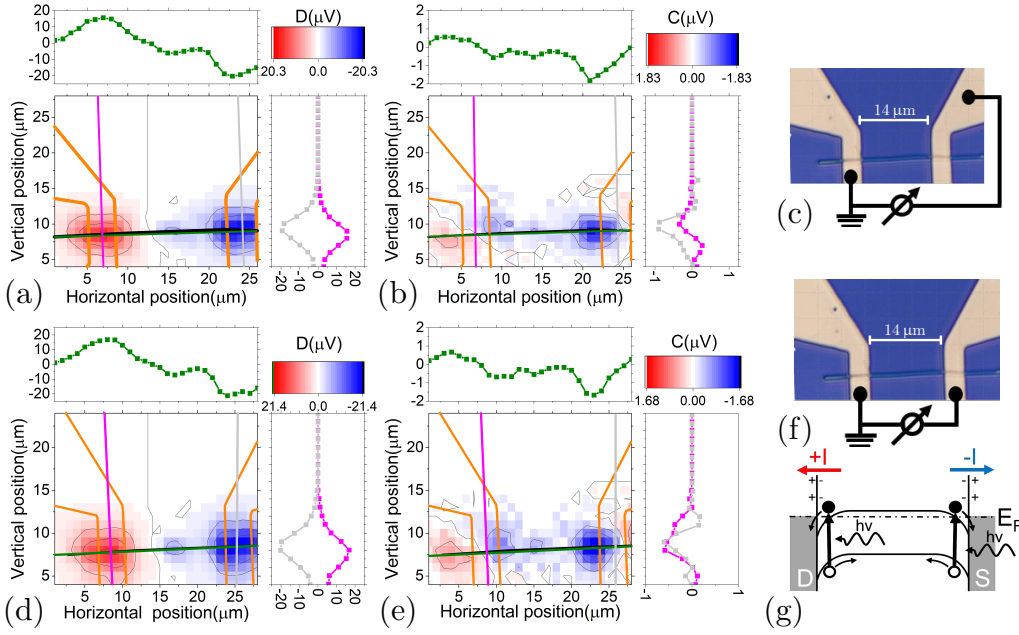


FIG. 3. Photovoltage measurements on a Bi_2Se_3 nanowire for different contacts. In (a), the thermovoltage map and in (b), the spin-polarized voltage map for the axisymmetric contacts are displayed. In (c), the axisymmetric position of the bond contacts is marked in black on a micrograph of the sample. In (d), the thermovoltage map and in (e), the spin-polarized voltage map are displayed for point-symmetric contacts. The bond contact position is marked in (f) on a micrograph of the sample. The contour plots along the nanowire (green lines) and along the contacts (pink and grey lines) are displayed next to the voltage maps. In (g), the influence of the band bending at the contact/nanowire interface on the photoelectrons is illustrated.

gradient. At the edges, one spin species is limited in its movement, which increases the optical induced asymmetric population of the surface states at the contact edges. This leads to an increase of the spin-polarized current at the contact edges on top of the nanowire. Hence we observe a positive (negative) spin-polarized current on the left (right) side of the drain electrode and zero spin-polarized current where the nanowire crosses the center of the contact (see FIG. 3(e)). At the source electrode, the temperature gradient is negative compared to the drain electrode (see FIG. 3(a)). Hence we expect a similar distribution of the spin-polarized current with the opposite sign, i.e. we expect a positive (negative) spin-current at the right side (left) of the source electrode, which matches the spin-polarized voltage at the source electrode in FIG. 3(e).

In summary, spatially resolved photocurrent measurements on Bi_2Se_3 nanowires were performed, focusing on the influence of the contact/nanowire interface on the thermovoltage and the spin-polarized current. Photocurrent measurements on several nanowires yield qualitatively similar results. The thermovoltage enhancement on the contact/nanowire interface is due to the Seebeck effect at the metal/semiconductor/metal junction and the band bending at the contact/nanowire interface. The Seebeck effect explains the thermovoltage gradient along the nanowire. The acceleration of the photoelectrons generated in the space charge region of the con-

tact/nanowire interface causes the enhancement and, in combination with the Gaussian profile of the laser light, the radial symmetry of the thermovoltage centered at the nanowire contact crossing. We observe for the spin-polarized voltage a constant region in the middle of the nanowire and an enhancement together with a dipole-like distribution of spin-polarized voltage at the contact edges. The spin-polarized voltage distribution is caused by the spin Nernst effect. We show that the influence of the gold contacts to the overall behavior of the nanowire is significant. The enhancement of the spin-polarized current, created in the vicinity of the contact pads, is in good agreement with the findings reported by Seifert et al.¹³. However, in our low excitation regime, the enhancement is caused by band-bending effects at the contact/nanowire interface and the spin Nernst effect. Enhancing spin-polarized currents in TI nanowires opens up new possibilities for spin current engineering, e.g. generating circular polarized THz radiation by crossed nanowires.

We are grateful to the German Science Foundation (DFG) for financial support through the priority program SPP1666: ‘Topological insulators: materials, fundamental properties, devices’ (MU1780/10-2).

Data availability

The data that support the findings of this study are available from the corresponding author upon reasonable request.

- ¹D. J. Thouless, M. Kohmoto, M. P. Nightingale, and M. den Nijs, “Quantized Hall Conductance in a Two-Dimensional Periodic Potential,” *Phys. Rev. Lett.* **49**, 405–408 (1982).
- ²C. L. Kane and E. J. Mele, “ Z_2 Topological Order and the Quantum Spin Hall Effect,” *Phys. Rev. Lett.* **95**, 146802 (2005).
- ³M. König, S. Wiedmann, C. Brüne, A. Roth, H. Buhmann, L. W. Molenkamp, X.-L. Qi, and S.-C. Zhang, “Quantum Spin Hall Insulator State in HgTe Quantum Wells,” *Science* **318**, 766–770 (2007).
- ⁴M. Z. Hasan and C. L. Kane, “Colloquium: Topological insulators,” *Rev. Mod. Phys.* **82**, 3045–3067 (2010).
- ⁵D. Hsieh, D. Qian, L. Wray, Y. Xia, Y. S. Hor, R. J. Cava, and M. Z. Hasan, “A topological Dirac insulator in a quantum spin Hall phase,” *Nature* **452**, 970–974 (2008).
- ⁶H. Zhang, C.-X. Liu, X.-L. Qi, X. Dai, Z. Fang, and S.-C. Zhang, “Topological insulators in Bi₂Se₃, Bi₂Te₃ and Sb₂Te₃ with a single Dirac cone on the surface,” *Nature Physics* **5**, 438–442 (2009).
- ⁷Y. Xia, D. Qian, D. Hsieh, L. Wray, A. Pal, H. Lin, A. Bansil, D. Grauer, Y. S. Hor, R. J. Cava, and M. Z. Hasan, “Observation of a large-gap topological-insulator class with a single dirac cone on the surface,” *Nature Physics* **5**, 398–402 (2009).
- ⁸Y. Yan, Z.-M. Liao, X. Ke, G. Van Tendeloo, Q. Wang, D. Sun, W. Yao, S. Zhou, L. Zhang, H.-C. Wu, and D.-P. Yu, “Topological Surface State Enhanced Photothermoelectric Effect in Bi₂Se₃ Nanoribbons,” *Nano Letters* **14**, 4389–4394 (2014).
- ⁹A. Sharma, B. Bhattacharyya, A. K. Srivastava, T. D. Senguttuvan, and S. Husale, “High performance broadband photodetector using fabricated nanowires of bismuth selenide,” *Scientific Reports* **6**, 19138 (2016).
- ¹⁰S. D. Ganichev and W. Prettl, “Spin photocurrents in quantum wells,” *Journal of Physics: Condensed Matter* **15**, R935–R983 (2003).
- ¹¹J. W. McIver, D. C. Hsieh, H. Steinberg, P. Jarillo-Herrero, and N. Gedik, “Control over topological insulator photocurrents with light polarization,” *Nature nanotechnology* **72**, 96–100 (2011).
- ¹²C. Kastl, C. Karnetzky, H. Karl, and A. W. Holleitner, “Ultrafast helicity control of surface currents in topological insulators with near-unity fidelity,” *Nature Communications* **6**, 6617 (2015).
- ¹³P. Seifert, K. Vaklinova, K. Kern, M. Burghard, and A. Holleitner, “Surface State-Dominated photoconduction and THz Generation in Topological Bi₂Te₂Se Nanowires,” *Nano Letters* **17**, 973–979 (2017).
- ¹⁴H. S. Shin, B. Hamdou, H. Reith, H. Osterhage, J. Gooth, C. Damm, B. Rellinghaus, E. Pippel, and K. Nielsch, “The surface-to-volume ratio: a key parameter in the thermoelectric transport of topological insulator Bi₂Se₃ nanowires,” *Nanoscale* **8**, 13552–13557 (2016).
- ¹⁵J. Gooth, J. G. Gluschke, R. Zierold, M. Leijnse, H. Linke, and K. Nielsch, “Thermoelectric performance of classical topological insulator nanowires,” *Semiconductor Science and Technology* **30**, 015015 (2014).
- ¹⁶V. A. Shalygin, H. Diehl, C. Hoffmann, S. N. Danilov, T. Herrle, S. A. Tarasenko, D. Schuh, C. Gerl, W. Wegscheider, W. Prettl, and S. D. Ganichev, “Spin photocurrents and the circular photon drag effect in (110)-grown quantum well structures,” *JETP Letters* **84**, 570–576 (2007).
- ¹⁷S. Luo, L. He, and M. Li, “Spin-momentum locked interaction between guided photons and surface electrons in topological insulators,” *Nature Communications* **8**, 2141 (2017).
- ¹⁸P. Olbrich, L. E. Golub, T. Herrmann, S. N. Danilov, H. Plank, V. V. Bel’kov, G. Mussler, C. Weyrich, C. M. Schneider, J. Kampmeier, D. Grützmacher, L. Plucinski, M. Eschbach, and S. D. Ganichev, “Room-temperature high-frequency transport of Dirac fermions in epitaxially grown Sb₂Te₃- and Bi₂Te₃- based topological insulators,” *Phys. Rev. Lett.* **113**, 096601 (2014).
- ¹⁹H. Plank, L. E. Golub, S. Bauer, V. V. Bel’kov, T. Herrmann, P. Olbrich, M. Eschbach, L. Plucinski, C. M. Schneider, J. Kampmeier, M. Lanius, G. Mussler, D. Grützmacher, and S. D. Ganichev, “Photon drag effect in (Bi_{1-x}Sb_x)₂Te₃ three-dimensional topological insulators,” *Phys. Rev. B* **93**, 125434 (2016).
- ²⁰N. Meyer, K. Geishendorf, J. Walowski, A. Thomas, and M. Münzenberg, “Photocurrent measurements in topological insulator Bi₂Se₃ nanowires,” *Applied Physics Letters* **116**, 172402 (2020), <https://doi.org/10.1063/1.5142837>.
- ²¹F. Léonard, E. Song, Q. Li, B. Swartzentruber, J. A. Martinez, and G. T. Wang, “Simultaneous Thermoelectric and Optoelectronic Characterization of Individual Nanowires,” *Nano Letters* **15**, 8129–8135 (2015), pMID: 26529491.
- ²²T. Schumann, N. Meyer, G. Mussler, J. Kampmeier, D. Grützmacher, E. Schmoranzero, L. Braun, T. Kampfrath, J. Walowski, and M. Münzenberg, “Observation of spin Nernst photocurrents in topological insulators,” , arXiv:1810.12799 (2018).